High-resolution x-ray spectroscopic study of the electronic structure of the prototypical *p*-type transparent conducting oxide $CuAlO_2$

D. J. Aston, D. J. Payne, A. J. H. Green, and R. G. Egdell*
Department of Chemistry, Inorganic Chemistry Laboratory, South Parks Road, Oxford OX1 3QR, United Kingdom

D. S. L. Law
National Centre for Electron Spectroscopy and Surface Analysis, Daresbury Laboratory, Warrington, Cheshire WA4 4AD, United Kingdom

J. Guo
Advanced Light Source, Lawrence Berkeley National Laboratory, Berkeley, California 94720, USA

P. A. Glans, T. Learmonth, and K. E. Smith
Department of Physics, Boston University, 590 Commonwealth Avenue, Boston, Massachusetts 02215, USA
(Received 20 July 2005; published 28 November 2005)

The electronic structure of the prototypical *p*-type transparent conducting oxide $CuAlO_2$ has been studied by O K and Cu L_3 shell x-ray absorption and emission and Al $K\alpha$ excited x-ray photoemission spectroscopy. The nonresonant O K shell emission is dominated by the O 2*p* partial density of states, while the Al $K\alpha$ excited valence photoemission and nonresonant Cu L_3 emission spectra are dominated by the Cu 3*d* partial density of states. All three techniques reveal mixing between O 2*p* and Cu 3*d* states. Cu L_3 emission spectra excited just above the L_3 threshold are dominated by inelastic scattering with 5.5 eV energy loss. This energy is shown to correspond to the separation between the dominant peaks in the filled and empty densities of states.

DOI: 10.1103/PhysRevB.72.195115 PACS number(s): 71.20.−b, 79.60.Bm, 78.70.En, 78.70.Dm

I. INTRODUCTION

The race to exploit transparent conducting oxides in electronic and optoelectronic devices such as ultraviolet (UV) emitting diodes and solid state lasers demands access to material that can be doped reproducibly both *n*-type or *p*-type. The best established transparent conducting oxides such as SnO_2, In_2O_3, or ZnO are easily doped *n*-type,[1] but the issue of whether these materials can also be doped *p*-type is still controversial.[2–4] Against this background, the discovery of a family of transparent *p*-type conducting ternary Cu(I) oxides has aroused widespread interest. *P*-type conductivity in these oxides was observed in the delafossite $CuAlO_2$[5,6] followed later by $CuGaO_2$ (Ref. 7) and $CuInO_2$.[8,9] More recently a range of other *p*-type conducting oxides including $SrCu_2O_2$ (Refs. 10 and 11) have appeared. However, $CuAlO_2$ remains as the prototype and most extensively studied oxide in this area.

The rhombohedral ($R\bar{3}m$) structure of $CuAlO_2$ is based on linear O-Cu-O dumbbells separated by sheets of AlO_6 octahedra in which the aluminum ions occupy the octahedral holes between layers of close packed oxygen ions (Fig. 1). Both the Al and Cu ions are therefore also found in hexagonal layers. The basic stacking sequence in the rhombohedral *R*3 polymorph is ABCABC: in the alternative hexagonal 2*H* polymorph the stacking sequence is ABAB. The local coordination around copper is similar to that in Cu_2O (cuprite). Within both structures there are strong interactions between Cu 3*d* and O 2*p* states of local σ symmetry, to give bonding levels of dominant O 2*p* character and antibonding states of dominant Cu 3*d* character. The admixture of some O 2*p* character into the Cu 3*d* states at the top of the valence band is believed to be important in reducing the effective mass of the hole states introduced by *p*-type doping. An important difference between the two oxides is that in cuprite the linear O-Cu-O units are connected in three dimensions in a structure based on two interpenetrating anti-SiO_2 nets, whereas in $CuAlO_2$ the O-Cu-O units are isolated. It has been argued that the reduced dimensionality of the Cu-Cu interactions is of central importance in determining that the bandgap of $CuAlO_2$ (originally quoted as 3.5 eV) is wider than that in Cu_2O (2.1 eV).[6,12] However, more recent experimental and theoretical work suggests that $CuAlO_2$ has an *indirect* gap of 1.8 eV.[11,13] This is actually smaller than the lowest bandgap of Cu_2O (which is *direct*). However the presence of an indirect gap as small as 1.8 eV has itself been called into ques-

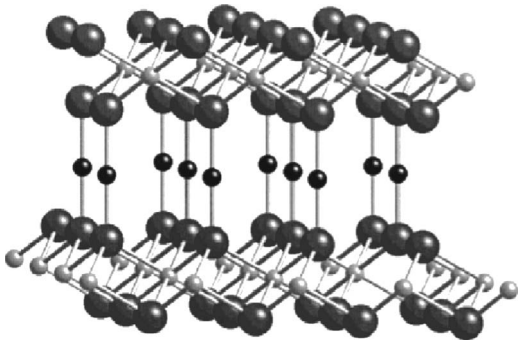

FIG. 1. The delafossite structure of $CuAlO_2$. Small black spheres are Cu, small gray spheres are Al. The larger spheres are O. Note the linear coordination of Cu.

tion. Using a hybrid Becke three parameter Lee-Yang-Parr (B3LYP) Hamiltonian, Robertson *et al.*[14] calculated that the lowest energy direct and indirect bandgaps were 4.5 and 3.9 eV, respectively. This computational approach gives reliable values of the bandgap for a wide range of materials including oxides,[15] and the calculations seem incompatible with a gap as small as 1.8 eV. It was, therefore, suggested that the 1.8 eV excitation relates to defects of some sort.[14]

We report here a comprehensive study of the electronic structure of $CuAlO_2$ using high resolution x-ray photoemission spectroscopy (XPS), x-ray emission spectroscopy (XES), and x-ray absorption spectroscopy (XAS). The valence band XPS spectra is dominated by the Cu 3*d* partial density of states, whereas the valence band O K-edge XES spectra is dominated by the O 2*p* partial density of states. These two techniques thus provide complementary approaches to investigation of the interaction between Cu 3*d* and O 2*p* states.

Bulk ceramic samples of $CuAlO_2$ prepared by conventional solid state synthetic procedures and thin films deposited by pulsed laser deposition are invariably *p*-type even without intentional doping. The mechanism for doping remains unclear. Holes are introduced into the upper part of the valence band by oxidation of the Cu^+ formally found in stoichiometric $CuAlO_2$ to the Cu^{2+} state. This may be achieved either by cation deficiency or incorporation of oxygen interstitials. Alternatively it is possible to envisage introduction of holes by substitution of divalent cations on the Al^{3+} sites. It should be noted, however, that a dopant ion such as Zn^{2+} will act as donor rather than an acceptor if it occupies a Cu^+ site rather than an Al^{3+} site.[16] A secondary objective of the present paper is to investigate the nature of the acceptor states in $CuAlO_2$ and to explore the possibility of *p*-type doping by replacement of Al by Zn.

II. EXPERIMENTAL

Ceramic samples of nominally undoped $CuAlO_2$ were prepared by reaction between CuO and Al_2O_3.[17,18] The precursor powders were mixed intimately in an agate mortar and pestle and pressed between 13 mm diameter tungsten carbide dies at 7 tons. Pellets were fired in air for three days at 1200 °C in recrystallized alumina boats and then quenched rapidly in liquid nitrogen. The samples were then reground, repelletized and refired at 1200 °C. They were finally quenched again in liquid nitrogen. The quenching step is crucial if the synthesis is carried out in air, since between 1000 °C and 612 °C, $CuAlO_2$ is thermodynamically unstable with respect to oxidation to $CuAl_2O_4$ and CuO, and below 612 °C to CuO and Al_2O_3. Zn doped samples with nominal composition $CuAl_{1-x}Zn_xO_2$ ($0<x<0.05$) were prepared by replacing an appropriate fraction of Al_2O_3 with ZnO. Oxidation of the doped samples proved to be highly problematic and it was necessary to perform a final firing at 1200 °C under flowing argon. The ceramic samples all gave clean powder diffraction patterns containing only sharp peaks associated with the rhombohedral ($R\bar{3}m$) delafossite phase. The samples were further characterized by four probe conductivity measurements, SQUID magnetometry, and electron spin resonance spectroscopy.

High-resolution x-ray photoemission spectra were measured in a Scienta ESCA 300 spectrometer. This incorporates a rotating anode Al $K\alpha$ ($h\nu=1486.6$ eV) x-ray source, a 7 crystal x-ray monochromator and a 300 mm mean radius spherical sector electron energy analyzer with parallel electron detection system. The x-ray source was run with 200 mA emission current and 14 kV anode bias, while the analyzer operated at 150 eV pass energy with 0.8 mm slits. Gaussian convolution of the analyzer resolution with a linewidth of 260 meV for the x-ray source gives an effective instrument resolution of 350 meV. Samples were mounted on molybdenum plates and cleaned in the preparation chamber of the XPS system by rear face electron beam heating in UHV to a temperature of 600 °C for 45 min. This reduced the C 1*s* to O 1*s* intensity ratio to below 1/100. Binding energies were referenced to the Fermi level of a silver sample regularly used to calibrate the spectrometer.

X-ray absorption and emission spectra were measured at beamline 7.0.1 at the advanced light source (ALS), Lawrence Berkeley National Laboratory. This beamline is equipped with a spherical grating monochromator.[19] Emission spectra were recorded using a Nordgren-type grazing-incidence spherical grating spectrometer.[20] For resonant emission experiments, the beamline was set to have an energy resolution of 350 meV at the O K edge and 750 meV at the Cu L_3 edge, and the emission spectrometer was set to have a resolution of 360 meV for O K and 700 meV for Cu L_3 edge spectra. Absorption spectra were measured in total electron yield (TEY) mode by monitoring the sample drain current. For the absorption measurements, the beamline resolution was set to 200 meV for the O K edge and to 500 meV for the Cu L_3 edge. The absorption spectra were normalized to a reference current from a clean gold mesh positioned in the path of the photon beam.

III. RESULTS AND DISCUSSION

A. The occupied density of states

The x-ray excited valence band photoemission spectrum of $CuAlO_2$ is shown in Fig. 2(a), while the cross section weighted density of states derived from the bandstructure calculations of Robertson *et al.* is shown in Fig. 2(b).[14] The calculations were based on a density functional approach using the generalized gradient approximation (GGA) and gave results in broad agreement with the published bandstructure calculations of Yanagi *et al.*[6] and Buljan *et al.*[21] The overall width of the valence band found experimentally is greater than that derived from the calculations. The tendency of density functional methods to "compress" the spread of energy levels as compared with experiment is widely recognized.[15,22] The one-electron cross sections for ionization of the valence orbitals contributing significantly to the occupied states are as follows:[23] Cu 3*d* 1.2×10^{-3} mB; Cu 4*s* 2.7×10^{-4} mB; O 2*p* 6.0×10^{-5} mB; Al 3*s* 3.9×10^{-4} mB; Al 3*p* 5.9×10^{-5} mB. Thus the cross section weighted density of states is dominated by the Cu 3*d* contribution, although the contribution from the O 2*p* and Al 3*s* partial

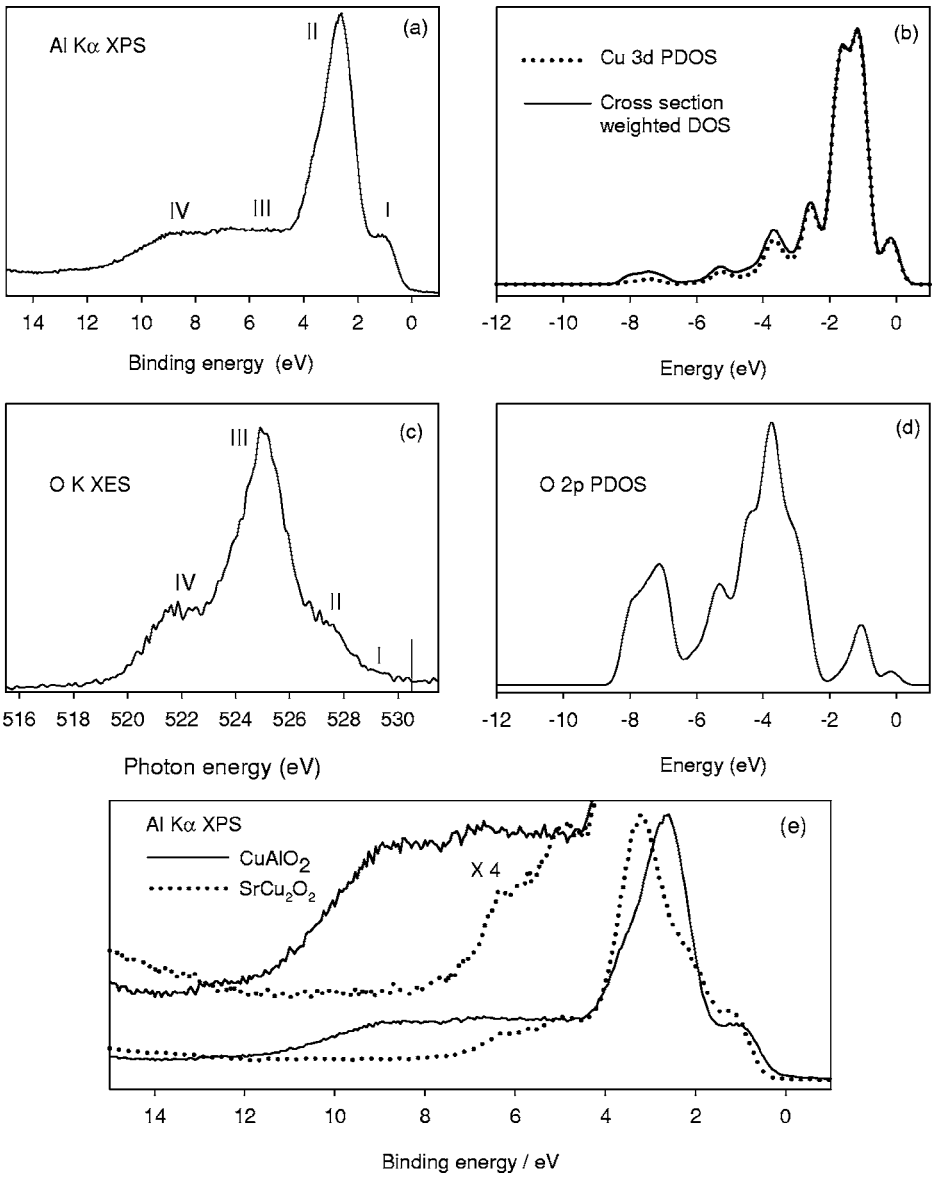

FIG. 2. (a) Valence band Al $K\alpha$ XPS of $CuAlO_2$. (b) Cross section weighted filled density of states and Cu 3*d* partial density of states. (c) O K shell emission of $CuAlO_2$. The alignment of this panel relative to the XPS data in (a) is established by the O 1*s* binding energy which is indicated by a short vertical line. (d) Filled O 2*p* partial density of states. The data in (c) and (d) are taken from the calculations of Robertson and coworkers. Note that (a) and (c) span an energy range of 16 eV, whereas the energy range in (b) and (d) is only 13 eV. (e) Comparison between valence band Al $K\alpha$ XPS of $CuAlO_2$ and $SrCu_2O_2$.

density of states (PDOS) is not entirely negligible, especially toward the bottom of the valence band. The experimental spectrum may be described in terms of four bands labeled I–IV in order of increasing binding energy. The relatively weak peak at onset I and the stronger band II (which has a distinct shoulder to low binding energy) are of dominant Cu 3*d* atomic character. The broader and weaker bands III and IV found at higher binding energy are by contrast of dominant O 2*p* atomic character, but the intensity of these peaks in XPS derives mainly from the Cu 3*d* character introduced into the O 2*p* bands by Cu 3*d*–O 2*p* mixing. The oxygen K shell emission excited under nonresonant conditions with photon energies well above the O K-edge absorption threshold provides a complementary view of the electronic structure, since the O K-edge XES spectra are dominated by the O 2*p* PDOS due to strong dipole selection rules for the decay of the core hole. Figure 2(c) presents the measured O K-edge XES spectrum reflecting the O 2*p* PDOS, while Fig. 2(d) presents the calculation of this PDOS. The Cu 3*d* bands I and II appear as weak features in the O K-edge XES spectrum, and are only observed due to mixing with the O 2*p* states; the spectrum is dominated by band III. The states at the bottom of the valence band are more strongly mixed with Cu 3*d* and Al 3*s* states and thus the intensity of band IV relative to band III is weaker in O K shell XES than in XPS. Overall there is excellent agreement between the calculated O 2*p* PDOS and the observed K shell emission spectrum.

The experimental valence band XPS of $CuAlO_2$ is compared with that of $SrCu_2O_2$ in Fig. 2(e).[24] $SrCu_2O_2$ is also a *p*-type transparent conducting oxide, and the Cu 3*d* bands in both materials have a similar appearance. Both are in turn similar to those in Cu_2O.[25] This may be traced to the fact that all three structures are based on linear O-Cu-O units. Within these linear groups the Cu $3d_z^2$ orbitals have σ-like symmetry, $3d_{xz}$ and $3d_{yz}$ π-like symmetry and $3d_{xy}$ and $3d_{x^2-y^2}$ δ-like symmetry.[12,24] Thus O 2*p* orbitals can mix with Cu $3d_z^2$ via strong σ overlap and with $3d_{xz}$ and $3d_{yz}$ via weaker π interactions. However $3d_{xy}$ and $3d_{x^2-y^2}$ must remain localized on Cu as there are no orbitals on oxygen of the correct δ symmetry for covalent mixing. Since the mixing arises

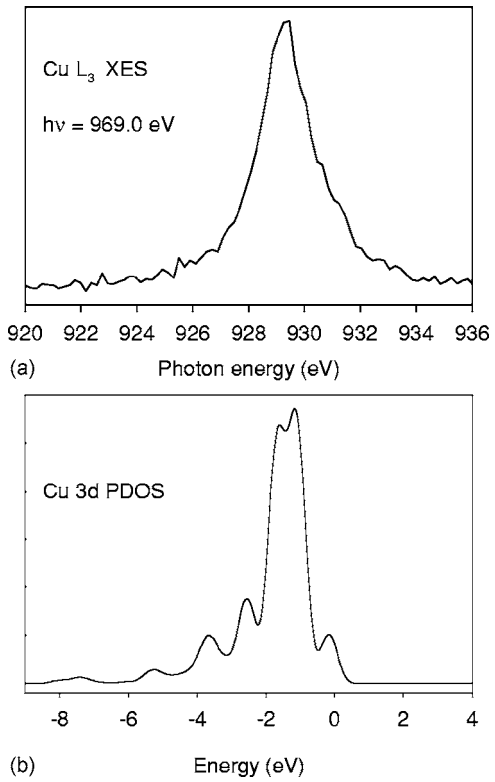

FIG. 3. (a) Nonresonant Cu L_3 x-ray emission spectrum of $CuAlO_2$ excited at 969.0 eV photon energy. (b) Occupied Cu 3*d* partial density of states derived from the bandstructure calculation of Robertson and co-workers. Note that the energy range in (a) is 16 eV whereas the energy range in (b) is only 13 eV.

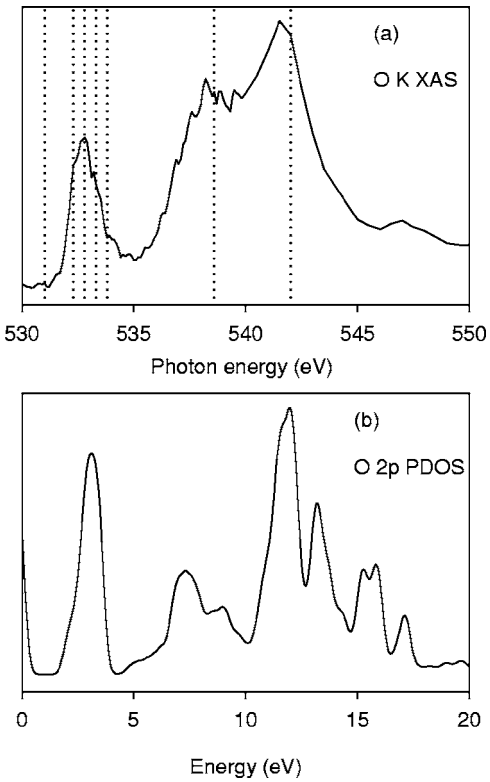

FIG. 4. (a) O K shell x-ray absorption spectrum of $CuAlO_2$. The vertical dotted lines indicate the photon energies used in excitation of resonant x-ray emission spectra. (b) Empty state O 2*p* partial density of states taken from the calculation of Robertson and co-workers.

from bonding-antibonding interactions between more tightly bound O 2*p* and less tightly bound Cu 3*d* states, we may qualitatively assign band I to the antibonding Cu 3*d* σ states and band II to the Cu 3*d* π and δ states. In $SrCu_2O_2$ the electronic structure within the O 2*p* bands mirrors that in the Cu 3*d* states: more strongly bonding σ states are found at higher binding energy than more weakly bonding π states.[24] The Sr 5*s* and 5*p* contribution to the occupied states is essentially negligible.[14] The situation for $CuAlO_2$ is more complex because the Al 3*s* and 3*p* contribution to the valence band states in $CuAlO_2$ cannot be ignored and strong Al-O interactions give rise to an O 2*p* bandwidth which is much greater in $CuAlO_2$ than in $SrCu_2O_2$.

Finally we can use Cu L shell emission as an alternative approach to characterizing the Cu 3*d* PDOS. The Cu L_3 x-ray emission spectrum of $CuAlO_2$ excited well above the absorption threshold is shown in Fig. 3. The spectrum consists of a single peak with broad wings. In principle the radiative decay spectrum contain contributions from both the Cu 4*s* and Cu 3*d* partial density of states, but the matrix elements connecting the Cu 2*p* core hole with the Cu 4*s* states are expected to be very much smaller than the corresponding matrix elements for Cu 3*d* states.[26] The figure, therefore, makes comparison between the experimental data and the Cu 3*d* partial density of states calculated by Robertson *et al.*[14] The correspondence between the two is quite good, although in contrast to the valence band XPS data, the low binding energy Cu 3*d* state peak I is not clearly resolved. It also appears that the O 2*p* valence band peaks III and IV make a smaller contribution to the x-ray emission spectrum than to the x-ray photoemission spectrum. This is to be expected. Whereas Cu L_3 XES depends only on the Cu 3*d* PDOS, the XPS experiment probes a cross section weighted density of states where contributions from the O 2*p* and Al 3*s* and 3*p* PDOS are small but not negligible.

B. X-ray absorption and resonant x-ray emission

The O K shell x-ray absorption spectrum of $CuAlO_2$ is shown in Fig. 4, along with the empty O 2*p* partial density of states derived from the bandstructure calculations of Robertson *et al.*[14] There is a sharp and well defined peak at a photon energy of about 532.5 eV [labeled (i) in the figure], just above threshold. This structure is very similar to that found in Cu_2O,[27] and is associated with antibonding conduction band states of mixed Cu 3*d*–O 2*p* character. There is also significant Cu 4*s* and 4*p* character in these states, although of course the spectral intensity in the O 1*s* absorption spectrum must derive from the O 2*p* contribution. The marked similarity between the absorption spectra of Cu_2O and $CuAlO_2$ in this region again reflects the fact that in both compounds the Cu has linear O-Cu-O coordination. This allows strong mutual mixing between Cu $3d_{z^2}$, Cu 4*s*, and O $2p_z$ orbitals, all of which have σ symmetry relative to the linear axis. Strong but broader peaks (ii) and (iii) are found at higher photon

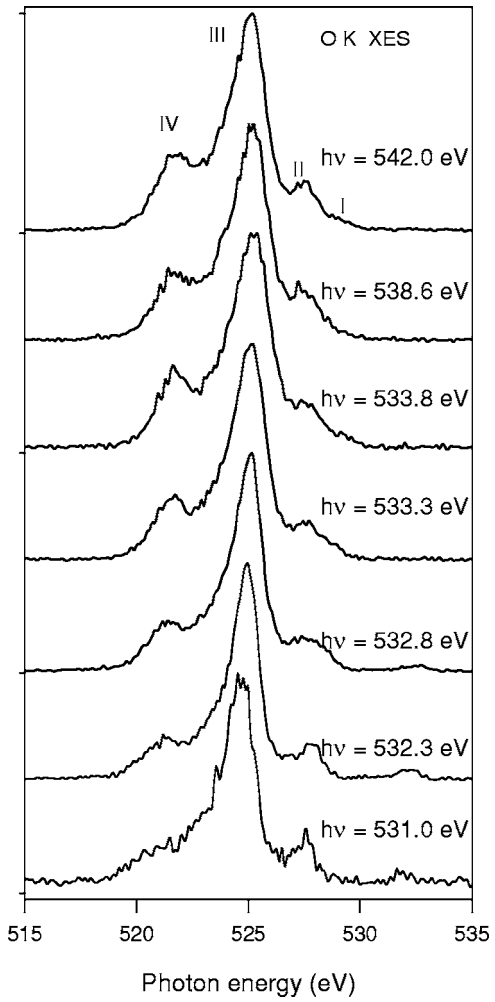

FIG. 5. O K shell x-ray emission spectra of $CuAlO_2$ excited at the near-threshold photon energies indicated.

energy with maxima at 538.6 and 541.5 eV. This structure is much more pronounced than in the corresponding spectrum of Cu_2O. It is associated with the antibonding states derived from strong mixing between O 2*p* and Al 3*s* and 3*p* states.

O K shell x-ray emission spectra excited close to threshold are shown in Fig. 5. The photon energies correspond to those indicated in Fig. 4. At the three lowest photon energies a weak peak due to elastic scattering may be observed, but in contrast to the Cu L_3 emission spectra to be discussed below, there is no indication of inelastic scattering features. The spectra are in fact broadly similar to those excited under nonresonant conditions well above the absorption threshold, although there are subtle variations in the intensities of features in the spectrum with varying photon energy. Of particular note is that the intensity of the peak IV associated with states at the bottom of the O 2*p* valence band is very low close to threshold but much higher at higher photon energy. The most tightly bound *occupied* valence band states responsible for peak IV have significant Al 3*s* character and the intensity enhancement appears to be related to the growth of Al 3*s* character in the *empty* states with increasing energy above threshold.

The Cu L_3 absorption spectrum of $CuAlO_2$ is shown in Fig. 6, along with empty Cu 3*d* and 4*s* partial densities of

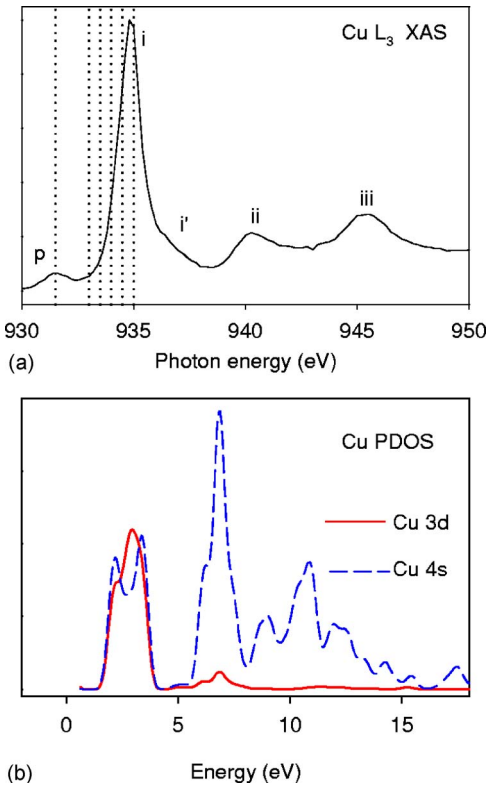

FIG. 6. (Color online) (a) Cu L_3 x-ray absorption spectrum of $CuAlO_2$. (b) Empty state Cu 3*d* and Cu 4*s* partial densities of states derived from the bandstructure calculations of Robertson and co-workers.

states derived from the bandstructure calculations of Robertson *et al.*[14] The spectrum is dominated by a strong threshold peak [labeled (i) in the figure] maximizing at a photon energy of 935.0 eV, with weaker peaks (ii) and (iii) at 940 and 946 eV, respectively. There is also a pronounced high energy shoulder *i′* to the threshold peak and a weak but well-defined pre-threshold peak labeled *p*. The leading peak again corresponds to the distinct maximum in the partial density of states, with mixed Cu 3*d*, 4*s*, and 4*p* and O 2*p* character. The main peak is at about 1.3 eV higher energy than found in Cu_2O.[27] Moreover the absorption onset is much less sharp and less intense (compared to the higher energy structure than in Cu_2O). In Cu_2O it is well established that the Cu L_3 threshold is strongly modified by the core hole potential which gives rise to a sharp threshold peak associated with a core hole exciton.[27] The excitonic contribution appears to be less important in $CuAlO_2$. This is possibly connected with the fact that $CuAlO_2$ has an indirect bandgap, whereas the gap of Cu_2O is direct. The pre-threshold peak is found at a photon energy of 931.5 eV. This is very close to the energy of the "main" peak in the x-ray absorption spectrum of CuO. We tentatively suggest that this peak is associated with hole states associated with oxidation of around 1% of the Cu to the divalent state, as will be discussed below.

Cu L_3 x-ray emission spectra of $CuAlO_2$ excited at the energy of the pre-peak *p* discussed above and at a further range of energies extending to the maximum of the absorption peak (i) are shown in Fig. 7. Under 931.5 eV excitation

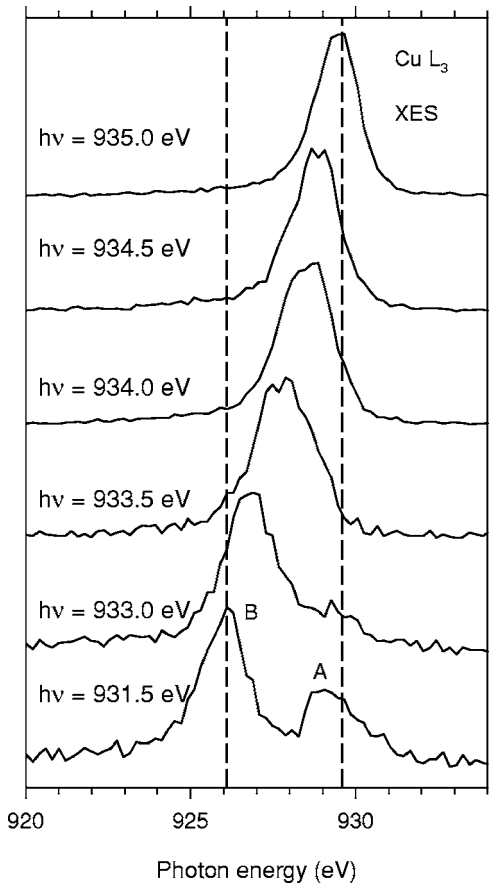

FIG. 7. Cu L_3 X-ray emission spectra of $CuAlO_2$ excited at the photon energies indicated. Note that the strongest spectral feature moves to higher energy with increasing photon energy, pointing to the fact that the spectra are dominated by inelastic scattering.

two peaks labeled *A* and *B* are observed. The stronger peak *A* moves to higher photon energy with increasing excitation energy. The overall shift in the peak maximum of band *A* from 926.1 to 929.6 eV as the photon energy increases from 931.5 to 935.0 eV exactly matches the change in exciting photon energy. Because the shift moves peak *B* toward *A*, the weaker peak *A* disappears under the envelope of *B* at photon energies above 933.0 eV. The position just below 930 eV of peak *A* determined from the spectrum excited at 931.5 eV photon energy matches the position of the emission maximum found under nonresonant excitation with 969.0 eV photons. Thus it appears that peak *A* corresponds to radiative decay from Cu 3*d* states into the $2p_{3/2}$ core hole. By contrast, peak *B* corresponds to inelastic electronic (i.e., Raman) scattering.[28] The energy loss is 5.4 eV. This energy corresponds to the separation between the peak II in the Cu-3*d* dominated density of states observed in XPS 3 eV below the top of the valence band and the maximum in the empty state peak (i) which lies about 2.5 eV above the valence band maximum in bandstructure calculations. As has already been discussed above, the empty state peak (i) contains substantial Cu 3*d*, Cu 4*s*, Cu 4*p*, and O 2*p* character. Thus the interband excitation has both charge transfer and *d-d* character, although it is not of course a *d-d* ligand field excitation in a conventional sense because Cu(I) has a formal configuration $3d^{10}$ with a full 3*d* shell.

C. The nature of the acceptor states and core level XPS

The activation energy for conduction in nominally undoped $CuAlO_2$ is about 0.22 eV. Thus the Fermi level is pinned by acceptor states just above the valence band maximum and the valence band onset found in Fig. 2 is just below the Fermi energy. The carrier concentration in thin films prepared by pulsed laser deposition (PLD) is of the order of 10^{17} cm^{-3}. Our magnetic susceptibility measurements on nominally undoped $CuAlO_2$ revealed an unpaired spin concentration corresponding to oxidation of about 1% of the Cu(I) to Cu(II). This may arise from oxygen interstitials or cation deficiency. The unpaired spin concentration remained at about 1% even after 5% Zn doping. Either Zn incorporation on Al sites is compensated by oxygen deficiency or Zn substitutes on both Cu and Al sites, which would lead to autocompensation. Whichever explanation is correct, the concentration of paramagnetic centers is seen to be much greater than the carrier concentration deduced from Hall measurements. Superficially this might be taken as evidence that the paramagnetism arises from impurity phases arising from oxidation of $CuAlO_2$, namely CuO and $CuAl_2O_4$. These would be difficult to detect by XRD at the 1% level. However, careful consideration of the structure in core level XPS provides evidence that argues against this possibility.

The core photoelectron spectra of nominally undoped and 5% Zn-doped $CuAlO_2$ in the region of Cu $2p_{3/2}$ core level are shown in Figs. 8(a) and 8(b), while a scan across the complete Cu 2*p* and Zn 2*p* region for the doped material is shown in Fig. 8(c).

The Cu 2*p* spectra are dominated by a simple spin-orbit slit doublet. The $2p_{3/2}$ component [labeled m1 in Fig. 8(b)] is found at 932.5(5) eV binding energy and has a full width at half maximum (FWHM) of only 1.04 eV. This corresponds to a Cu $3d^{10}$ configuration in the final state arising from Cu(I). A broader (FWHM=2.06 eV) and weaker peak m2 also corresponds to Cu $3d^{10}$ final states, but this is now associated with the Cu(II) arising from introduction of holes into the Cu 3*d* bands.

The final state $3d^{10}$ configuration is derived from the Cu(II) $3d^9$ initial state configuration by screening of the core hole by transfer of an electron into the 3*d* orbital of the ionized atom.[25,28–30] In general for Cu(II) oxides it is possible to identify two different screening channels: a local channel involving charge transfer from a neighboring ligand (oxygen) site to give a final state configuration $2p^5 3d^{10}\underline{L}^1$ where $\underline{L}^1$ denotes a ligand hole and the other occupancies refer to the Cu site; and a nonlocal channel where the valence band hole delocalizes away from the ionized site to give Zhang-Rice singlet states.[31–33] Both screening channels operate in CuO;[31] and in Cu(II) oxyhalides such as $Sr_2CuO_2Cl_2$ and $Ba_3Cu_3O_4Cl_2$ where CuO_4 plaquettes are connected via corner sharing: the 180° Cu-O-Cu bond angle allows facile O mediated hole hopping.[32] By contrast it has been argued that the Zhang-Rice screening channel cannot operate in Cu 2*p* XPS of oxides such as Li_2CuO_2 where the CuO_4 plaquettes are connected in one-dimensional (1D) linear ribbons via edge sharing. Here the Cu-O-Cu bond angle is 90° and O mediated hole hopping between Cu sites is suppressed. The Cu coordination in $CuAlO_2$ differs from that

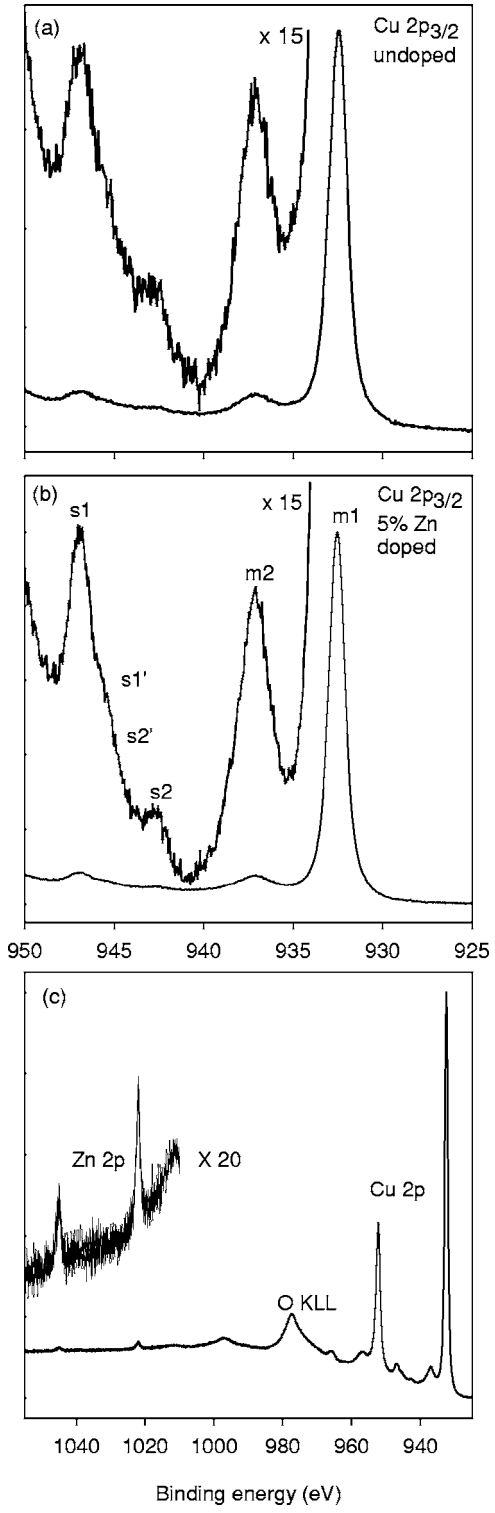

FIG. 8. Al $K\alpha$ XPS in the Cu $2p_{3/2}$ region (a) of nominally doped $CuAlO_2$ (b) of 5% Zn-doped $CuAlO_2$. (c) Wide scan across the complete Cu $2p$ Zn $2p$ region for 5% Zn-doped material.

of any Cu(II) oxide. However, it is evident that the O-Cu-O dumbbells are completely isolated from each other and only a local screening mechanism is possible. This accounts for the symmetric and relatively narrow line shape of the m2 peak of $CuAlO_2$: a similar peak shape is found for Li_2CuO_2

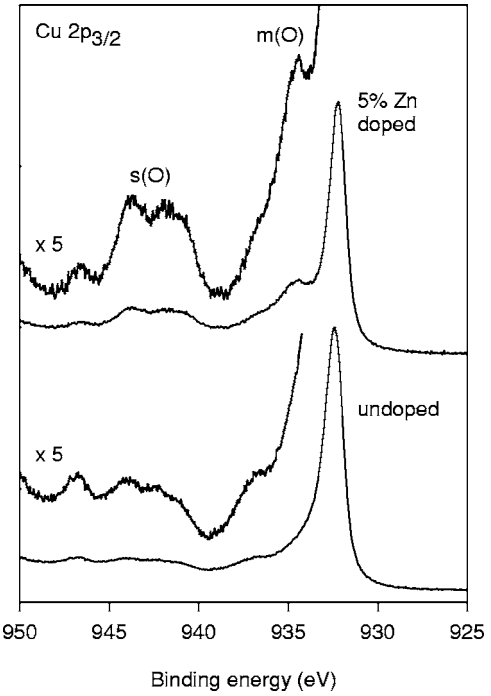

FIG. 9. Cu $2p_{3/2}$ core level structure in Al $K\alpha$ XPS of nominally undoped $CuAlO_2$ and 5% Zn-doped $CuAlO_2$ following oxidation in air at 700 °C for one hour.

where as has been discussed only local screening is possible.[32] The binding energy of the Cu(II) peak found in $CuAlO_2$—937.1 eV—is, however, very much higher than found for Li_2CuO_2, where the peak maximum is at 934.0 eV, or indeed for any other Cu(II) oxide. The binding energy is determined by the Coulombic interaction between the Cu $2p$ core level and the O $2p$ hole. This interaction should be much stronger in $CuAlO_2$ than in Li_2CuO_2 due to the lower coordination number and shorter Cu-O bond lengths: in $CuAlO_2$ the Cu-O bond length is only 1.86 Å whereas in Li_2CuO_2 the bond length is 1.96 Å.[34]

Satellites associated with $3d^9$ final states are labeled $s1$, $s1'$, $s2$, $s2'$ in Fig. 8(b). The first two satellites have binding energies of 946.9 and 945.0 eV. These energies are similar to those of weak satellites in Cu_2O arising from excitation of a Cu $3d$ electron into the conduction band to give a $2p^5 3d^9 \underline{L}^0 (4s, 4p)^1$ final state. The satellites $s2$ and $s2'$ at lower binding energy are associated with the $3d^9$ states derived from Cu(II). The $s1$ satellites are at higher binding energy than the $s2$ satellites because formation of Cu(I) d^9 satellites involves interband excitation, whereas $s2$ satellites are derived simply from removal of a core electron with retention of the initial state valence configuration.

In summary, the unusually high binding energy associated with peak m2 provides convincing evidence that it is not associated with simple Cu(II) oxidation products but arises from Cu(II) ions confined in what is essentially a Cu(I) site. This conclusion is reinforced by studies of oxidation of ceramic samples of undoped and doped samples of $CuAlO_2$. It was found that surface oxidation proceeds rapidly in air at temperatures around 700 °C and above. Figure 9 shows the effects of heating in air at this temperature for one hour.

There is clearly pronounced growth in the intensity of the Cu(II) d^9 satellites, identified as s(O) in the figure. This is accompanied by growth of Cu(II) d^{10} structure at a binding energy of around 934.40 eV, identified as m(O). This is within the range found for typical Cu(II) compounds and is to be associated with the $CuAl_2O_4$ and CuO which are the major oxidation products identified by XRD. It is striking that Zn doping $CuAlO_2$ leads to a material which oxidizes much more rapidly than the undoped material. This is again consistent with the hypothesis that Zn doping is partially compensated by O vacancies. These vacancies will increase the rate of oxygen ion transport and facilitate the oxidative degradation of the samples.

It is now possible to make comparison between the hole concentration seen in XPS and the unpaired spin concentration inferred from magnetic susceptibility measurements. The intensity ratio between the Cu(II) peak m2 and the Cu(I) peak m1 is about 0.097. Given that more of the spectral weight associated with Cu(II) resides in the $3d^9$ satellites than for Cu(I), this number sets a lower limit on the hole concentration (as a fraction of Cu sites) probed by XPS. The Cu(II) fraction probed by XPS is about a factor of 10 greater than the unpaired spin concentration (1%) derived from magnetic measurements. This implies pronounced accumulation of holes in the near-surface region. Taking account of a unit cell volume[35] of 119.74 Å^3 (Z=3), the 1% unpaired spin concentration in turn equates to a hole concentration of 2.5×10^{20} cm^{-3}. This is very much greater than the carrier concentrations of the order of 10^{17} cm^{-3} deduced from Hall effect measurements.[5,6] We must conclude that not all Cu(II) centers act as shallow acceptors. A similar situation pertains in K-doped $SrCu_2O_2$.[22]

IV. CONCLUDING REMARKS

X-ray absorption and emission and x-ray photoemission spectroscopies provide a consistent picture of the electronic structure of $CuAlO_2$ in broad agreement with bandstructure calculations. There is significant mixing between O 2p and Cu 3d states, revealed most directly in O K shell emission spectra. There is also significant mixing between Al 3s and O 2p states. This causes significant broadening of the lower part of the O 2p valence band as compared with $SrCu_2O_2$, where the Sr levels are not significantly involved in the occupied valence band states. Both Cu L shell x-ray absorption and Cu 2p photoemission spectra contain structure associated with Cu 3d valence band holes, with pronounced accumulation of holes in the near surface region. Zn doping does not increase the hole concentration.

ACKNOWLEDGMENTS

The Boston University (BU) program is supported in part by the Department of Energy under DE-FG02-98ER45680, and the National Science Foundation under DMR-0311792. The ALS is supported by the U.S. Department of Energy, Materials Sciences Division. The Oxford University programme is supported by EPSRC Grant No. GR/S94148 and the NCESS facility at Daresbury Laboratory by EPSRC Grant No. GR/S14252. We are grateful to Professor J. Robertson for making available the results of his bandstructure calculations.

*Corresponding author. Electronic mail: russell.egdell@chem.ox.ac.uk

[1] See, e.g., for a discussion of n-type doping in In_2O_3 C. G. Granqvist and A. Hultåker, Thin Solid Films **411**, 1 (2002).
[2] T. Yamamoto and H. K. Yoshida, Jpn. J. Appl. Phys., Part 2 **38**, L166 (1999).
[3] M. Joseph, H. Tabata, and T. Kawai, Jpn. J. Appl. Phys., Part 2 **38**, L1205 (1999).
[4] A. Tsukazaki, H. Saito, K. Tamura, M. Ohtani, H. Koinuma, M. Sumiya, S. Fuke, T. Fukumura, and M. Kawasaki, Appl. Phys. Lett. **81**, 235 (2002).
[5] H. Kawazoe, M. Yasukawa, H. Hyodo, M. Kurita, H. M. Yanagi, and H. Hosono, Nature (London) **389**, 939 (1997).
[6] H. Yanagi, S. Inoue, K. Ueda, H. Kawazoe, H. Hosono, and N. Hamada, J. Appl. Phys. **88**, 4159 (2000).
[7] K. Ueda, T. Hase, H. Yanagi, H. Kawazoe, H. Hosono, H. Ohta, M. Orita, and M. Hirano, J. Appl. Phys. **89**, 1790 (2001).
[8] H. Yanagi, H. Kawazoe, A. Kudo, M. Yasukawa, and H. Hosono, J. Electroceram. **4**, 407 (2000).
[9] H. Yanagi, T. Hase, S. Ibuki, K. Ueda, and H. Hosono, Appl. Phys. Lett. **78**, 1583 (2001).
[10] A. Kudo, H. Yanagi, H. Hosono, and H. Kawazoe, Appl. Phys. Lett. **73**, 220 (1998).
[11] H. Ohta, M. Orita, M. Hirano, I. Yagi, K. Ueda, and H. Hosono, J. Appl. Phys. **91**, 3074 (2002).
[12] A. Buljan, M. Llunell, E. Ruiz, and P. Alemany, Chem. Mater. **13**, 338 (2000).
[13] X. L. Xie, S. H. Wei, and S. B. Zhang, Phys. Rev. Lett. **88**, 066405 (2002).
[14] J. Robertson, P. W. Peacock, M. D. Towler, and R. Needs, Thin Solid Films **411**, 96 (2002).
[15] J. Muscat, A. Wander, and N. M. Harrison, Chem. Phys. Lett. **342**, 397 (2001).
[16] M. V. Lalic, J. Mestnik, A. W. Carbonari, and R. N. Saxena, Solid State Commun. **125**, 175 (2003).
[17] A. N. Banerjee, S. Kundoo, and K. K. Chattopadhyay, Thin Solid Films **440**, 5 (2003).
[18] K. T. Jacob and C. B. Alcock, J. Am. Ceram. Soc. **58**, 192 (1975).
[19] J. Nordgren and R. Nyholm, Nucl. Instrum. Methods Phys. Res. A **246**, 242 (1986).
[20] J. Nordgren, G. Bray, S. Cramm, R. Nyholm, J. E. Rubensson, and N. Wassdahl, Rev. Sci. Instrum. **60**, 1690 (1989).
[21] A. Buljan, P. Alemany, and E. Ruiz, J. Phys. Chem. B **103**, 8060 (1999).
[22] Y. Dou, R. G. Egdell, D. S. L. Law, N. M. Harrison, and B. G. Searle, J. Phys.: Condens. Matter **10**, 8447 (1998).
[23] J. J. Yeh and I. Lindau, At. Data Nucl. Data Tables **32**, 1 (1985).

[24] C. C. B. Lynch, R. G. Egdell, and D. S. L. Law, Chem. Phys. Lett. **401**, 223 (2005).
[25] J. Ghijsen, L. H. Tjeng, J. van Elp, H. Eskes, J. Westerink, G. A. Sawatzky, and M. T. Czyzyk, Phys. Rev. B **38**, 11322 (1988).
[26] U. Fano and J. W. Cooper, Rev. Mod. Phys. **40**, 441 (1968).
[27] M. Grioni, J. F. van Acker, M. T. Czyzyk, and J. C. Fuggle, Phys. Rev. B **45**, 3309 (1993).
[28] G. van der Laan, C. Westra, C. Haas, and G. A. Sawatzky, Phys. Rev. B **23**, 4369 (1981).
[29] K. Karlsson, O. Gunnarsson, and O. Jepsen, J. Phys.: Condens. Matter **4**, 2801 (1992).
[30] K. Karlsson, O. Gunnarsson, and O. Jepsen, Int. J. Mod. Phys. B **14**, 3791 (2000).
[31] M. A. van Veenendaal and G. A. Sawatzky, Phys. Rev. Lett. **70**, 2459 (1993).
[32] T. Bőske, K. Maiti, O. Knauff, K. Ruck, M. S. Golden, G. Krabbes, J. Fink, T. Osafune, N. Motoyama, H. Eisaki, and S. Uchida, Phys. Rev. B **57**, 138 (1998).
[33] A. Koitzsch, J. Fink, M. S. Golden, K. Karlsson, O. Jepsen, O. Gunnarsson, L. L. Miller, H. Eisaki, S. Uchida, G. Yang, and S. Abell, Phys. Rev. B **66**, 024519 (2002).
[34] F. Sapina, J. Rodriguez Carvajal, M. J. Sanhis, R. Ibanez, A. Beltran, and D. Beltran, Solid State Commun. **74**, 779 (1990).
[35] T. Ishiguro, Acta Crystallogr., Sect. B: Struct. Sci. **39**, 564 (1983).